arXiv:astro-ph/0612688v2 28 Jul 2008

Optimal filters on the sphere

Jason D. McEwen, Michael P. Hobson, and Anthony N. Lasenby

***Abstract*— We derive optimal filters on the sphere in the context of detecting compact objects embedded in a stochastic background process. The matched filter and the scale adaptive filter are derived on the sphere in the most general setting, allowing for directional template profiles and filters. The performance and relative merits of the two optimal filters are discussed. The application of optimal filter theory on the sphere to the detection of compact objects is demonstrated on simulated data. A naive detection strategy is adopted, with an initial aim of illustrating the application of the new filter theory derived on the sphere. Nevertheless, this simple object detection strategy is demonstrated to perform well, even at low signal-to-noise ratio.**

***Index Terms*— Filtering, spheres, convolution.**

I. Introduction

THE detection of compact objects embedded in a stochastic background is a problem experienced in many branches of physics and signal processing, and as such it has received considerable attention. Many of these applications are restricted to flat Euclidean space, such as the one-dimensional line or the two-dimensional plane. However, data are often measured or defined on other manifolds, such as the two-sphere. For example, applications where data are defined on the sphere are found in planetary science, geophysics, computer vision, quantum chemistry and astrophysics. Astrophysical applications include observations made on the celestial sphere of the cosmic microwave background (CMB) (*e.g.* [1]), a relic radiation of the Big Bang. CMB observations may be contaminated by localised foreground emission due to point sources or Sunyaev-Zel'dovich (SZ) effects induced by the hot intergalactic gas bound to clusters of galaxies [2]. These foreground emissions must be separated from CMB observations in order to provide cleaned CMB data for cosmological analysis or simply so that they may be studied in their own right. Furthermore, other primordial physical phenomena may imprint localised signatures in the CMB that are of interest (*e.g.* cosmic strings [3]). The extension of optimal filter theory to the sphere would allow compact objects embedded in full-sky CMB data to be detected in an analogous manner to that performed in the plane currently, *i.e.* by filtering the observed field to enhance the contribution of embedded objects relative to the stochastic background, before attempts are made to recover the embedded objects from the filtered field using various classification schemes.

When adopting the filtering approach to object detection a number of criteria may be imposed so that the filter kernels are in some sense optimal. The optimal matched filter (MF) has been used extensively in many branches of physics and signal processing, and in the context of detecting point sources and SZ emission in CMB observations made on small patches of the sky, which are assumed to be approximately flat, by [4] and [5] respectively. Other optimal filters in Euclidean space, such as the scale adaptive filter (SAF), have been derived by [6], [7]. It is shown by [6] that the Mexican hat wavelet on the plane is in fact the optimal SAF for the special case of detecting a Gaussian source embedded in a white noise background. The Mexican hat wavelet has been used to detect objects embedded in CMB data on small patches of the sky [8]. Furthermore, both the MF and SAF (including the Mexican hat wavelet) have been applied to simulated time ordered CMB data to detect point sources [9]. Some debate exists, however, over the advantage of the SAF relative to the usual MF [10].

All of the works discussed previously are limited to Euclidean space. To analyse full-sky CMB observations the techniques described previously must be extended to a spherical manifold. As a consequence of a full-sky analysis, it should be noted that the statistical properties of the background process are assumed to be stationary over the sphere. The Mexican hat wavelet analysis has been extended to the sphere and applied to point source detection in the CMB by [11]. The extension of optimal filter theory to the sphere has been derived recently by [12] and applied to simulated data to detect the SZ effect [13]. However, the optimal filter theory derived by [12] is restricted to azimuthally symmetric source profiles and filters on the sphere. In this paper we re-derive optimal filter theory on the sphere, making the extension to the more general class of non-azimuthally symmetric source profiles and filters. In addition, we generalise to L^p-norm preserving dilations in order to highlight some minor amendments to previous works.

The remainder of this paper is organised as follows. In Section II some mathematical preliminaries are presented before the object detection problem is formalised in Section III. Derivations of the MF and SAF on the sphere are presented in Section IV. In Section V the new optimal filter theory is applied to detect objects embedded in simulated data, in the MF case. Concluding remarks are made in Section VI.

II. Mathematical Preliminaries

It is necessary to outline some mathematical preliminaries before attempting to derive optimal filters on the sphere. Firstly, harmonic analysis on the two-sphere $\mathbb{S}^2$ and on the rotation group $\mathrm{SO}(3)$ is reviewed. By making all assumptions and definitions explicit we hope to avoid any confusion over the conventions adopted. A dilation operator is then defined on the sphere, before we review filtering on the sphere. Dilation and filtering are described in both real and harmonic space.

Manuscript received 26 January, 2007.

The authors are with the Astrophysics Group, Cavendish Laboratory, Cambridge, UK.

E-mail: mcewen@mrao.cam.ac.uk (J. D. McEwen)

A. Harmonic representations

We consider the space of square integrable functions $L^2(\mathbb{S}^2, \mathrm{d}\Omega(\omega))$ on the unit two-sphere $\mathbb{S}^2$, where $\mathrm{d}\Omega(\omega) = \sin\theta\,\mathrm{d}\theta\,\mathrm{d}\phi$ is the usual rotation invariant measure on the sphere and $\omega = (\theta, \phi) \in \mathbb{S}^2$ denotes spherical coordinates with colatitude θ and longitude ϕ. A square integrable function on the sphere $f \in L^2(\mathbb{S}^2, \mathrm{d}\Omega(\omega))$ may be represented by the spherical harmonic expansion $f(\omega) = \sum_{\ell=0}^{\infty}\sum_{m=-\ell}^{\ell} f_{\ell m} Y_{\ell m}(\omega)$, where the spherical harmonic coefficients are given by the usual projection on to the spherical harmonic basis functions: $f_{\ell m} = \int_{\mathbb{S}^2} f(\omega)\, Y^*_{\ell m}(\omega)\ \mathrm{d}\Omega(\omega)$. The $*$ denotes complex conjugation. We adopt the Condon-Shortley phase convention where the normalised spherical harmonics are defined by [14]

$$Y_{\ell m}(\omega) = (-1)^m \sqrt{\frac{2\ell+1}{4\pi}\frac{(\ell-m)!}{(\ell+m)!}}\, P_\ell^m(\cos\theta)\, \mathrm{e}^{\mathrm{i}m\phi}\ ,$$

where $P_\ell^m(x)$ are the associated Legendre functions. Using this normalisation the orthogonality of the spherical harmonic functions is given by

$$\int_{\mathbb{S}^2} Y_{\ell m}(\omega)\, Y^*_{\ell' m'}(\omega)\ \mathrm{d}\Omega(\omega) = \delta_{\ell\ell'}\delta_{mm'}\ , \tag{1}$$

where δ_{ij} is the Kronecker delta function.

To perform filtering on the sphere one must define translations on the sphere, which may be naturally represented by rotations. Rotations on the sphere $\mathcal{R}$ are characterised by the elements of the rotation group $\mathrm{SO}(3)$, which we parameterise in terms of the three Euler angles $\rho = (\alpha, \beta, \gamma) \in \mathrm{SO}(3)$, where $\alpha \in [0, 2\pi)$, $\beta \in [0, \pi]$ and $\gamma \in [0, 2\pi)$.[1] The rotation of f is defined by $[\mathcal{R}(\rho)f](\omega) \equiv f(R_\rho^{-1}\omega)$, where R_ρ is the rotation matrix corresponding to $\mathcal{R}(\rho)$. It is also useful to characterise the rotation of a function on the sphere in harmonic space. The harmonic coefficients of a rotated function are related to the coefficients of the original function by

$$[\mathcal{R}(\rho)f]_{\ell m} = \sum_{m'=-\ell}^{\ell} D^\ell_{mm'}(\rho)\, f_{\ell m'}\ . \tag{2}$$

The Wigner functions may be decomposed as [14]

$$D^\ell_{mm'}(\alpha,\beta,\gamma) = \mathrm{e}^{-\mathrm{i}m\alpha}\, d^\ell_{mm'}(\beta)\, \mathrm{e}^{-\mathrm{i}m'\gamma}\ , \tag{3}$$

where the real polar d-matrix is defined by [14]

$$d^\ell_{mm'}(\beta) = \sqrt{\frac{(\ell+m')!(\ell-m')!}{(\ell+m)!(\ell-m)!}}\left(\sin\frac{\beta}{2}\right)^{m'-m} \times \left(\cos\frac{\beta}{2}\right)^{m'+m} P^{(m'-m,m'+m)}_{\ell-m'}(\cos\beta)\ , \tag{4}$$

where $P_\ell^{(a,b)}(\cdot)$ are the Jacobi polynomials. The Wigner functions satisfy the orthogonality condition

$$\int_{\mathrm{SO}(3)} D^\ell_{mn}(\rho)\, D^{\ell'*}_{m'n'}(\rho)\ \mathrm{d}\varrho(\rho) = \frac{8\pi^2}{2\ell+1}\,\delta_{\ell\ell'}\delta_{mm'}\delta_{nn'}\ , \tag{5}$$

where $\mathrm{d}\varrho(\rho) = \sin\beta\,\mathrm{d}\alpha\,\mathrm{d}\beta\,\mathrm{d}\gamma$. Recursion formulae are available to compute rapidly the Wigner d-matrices (see *e.g.* [15]).

[1]We adopt the zyz Euler convention corresponding to the rotation of a physical body in a *fixed* co-ordinate system about the z, y and z axes by γ, β and α respectively.

B. Dilation on the sphere

To perform filtering on the sphere at various scales a spherical dilation operator must be defined. We adopt the spherical dilation operator first defined by [16] to derive a continuous wavelet transform on the sphere. In this case, the stereographic projection is used to project the sphere on to the plane (see Figure 1). It is shown by [17] that the stereographic projection operator is the unique unitary, radial and conformal diffeomorphism between the sphere and the plane. Dilations on the sphere are defined by: (a) first lifting the sphere to the plane using the stereographic projection; (b) performing the usual Euclidean dilation in the plane; (c) reprojecting back on to the sphere using the inverse stereographic projection. The spherical dilation operator derived by [16], [17] preserves the L^2-norm of functions. We generalise to L^p-norm preserving dilations in order to highlight the impact of this choice on the final optimal filter equations derived in Section IV. Although the choice of p is not of considerable practical interest, different works have implicitly assumed different p values, hence the explicit dependence given here should allow a direct comparison with previous works. Definitions of the dilation and inverse dilation (contraction) operators follow, accompanied by short proofs to show that these operators do indeed preserve the L^p-norm.

Definition 1: The L^p-norm preserving spherical dilation is defined by

$$f_{R,p}(\theta,\phi) \equiv [\mathcal{D}_p(R)f](\theta,\phi) \equiv [\lambda(R,\theta)]^{1/p}\, f(\theta_{1/R},\phi)\ , \tag{6}$$

where scale $R \in \mathbb{R}_*^+$, L^p-norm $p \in \mathbb{Z}_*^+$, $\tan(\theta_R/2) = R\tan(\theta/2)$ and the $\lambda(R,\theta)$ cocycle term introduced to preserve the appropriate norm is defined by

$$\lambda(R,\theta) = \frac{4\,R^2}{[(R^2-1)\cos\theta + (R^2+1)]^2}\ . \tag{7}$$

□

Proof: See Appendix I. ■

A contraction, or inverse spherical dilation, may be similarly defined and follows trivially from Definition 1.

Definition 2: The L^p-norm preserving inverse spherical dilation is defined by

$$[\mathcal{D}_p^{-1}(R)f](\theta,\phi) \equiv [\lambda(R,\theta_R)]^{-1/p}\, f(\theta_R,\phi)\ . \tag{8}$$

□

The spherical dilation and contraction operations are performed about the north pole. A dilation about any other point on the sphere may be performed by rotating that point to the north pole, dilating, then rotating back to the original position.

When constructing optimal filters on the sphere it is necessary to consider the spherical harmonic coefficients of dilated functions. We derive an intermediate result here to express the harmonic coefficients of the dilated function in terms of the original undilated function and dilated spherical harmonic functions.

Lemma 1: The harmonic coefficients of a dilated function may be given either by projecting the dilated function on

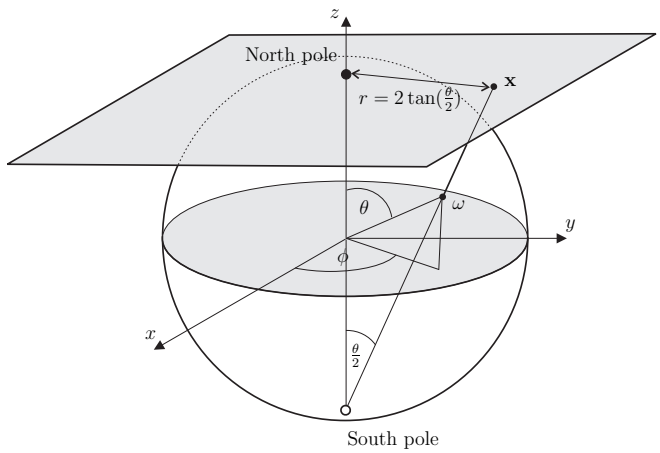

Fig. 1. Stereographic projection of the sphere on to the plane.

to each spherical harmonic, or equivalently by projecting the original undilated function on to contracted spherical harmonics, scaled by the appropriate cocycle factor:

$$[\mathcal{D}_p(R)f]_{\ell m} = \int_{\mathbb{S}^2} f(\theta,\phi)\, \frac{Y^*_{\ell m}(\theta_R,\phi)}{[\lambda(R,\theta_R)]^{1-1/p}}\, \mathrm{d}\Omega(\theta,\phi)\,. \quad (9)$$

Indeed, for the 2-norm case ($p=2$) one finds $1-1/p = 1/p$ and the spherical harmonics are contracted in accordance with the definition of the inverse dilation:

$$[\mathcal{D}_2(R)f]_{\ell m} = \int_{\mathbb{S}^2} f(\theta,\phi)\, [\mathcal{D}_2^{-1}(R) Y^*_{\ell m}](\theta,\phi)\ \mathrm{d}\Omega(\theta,\phi)\,.$$

□

Proof: Consider the spherical harmonic coefficients of a dilated function

$$[\mathcal{D}_p(R)f]_{\ell m} = \int_{\mathbb{S}^2} [\lambda(R,\theta)]^{1/p} f(\theta_{1/R},\phi) Y^*_{\ell m}(\theta,\phi)\, \mathrm{d}\Omega(\theta,\phi).$$

By performing a change of variables this may be represented by

$$[\mathcal{D}_p(R)f]_{\ell m} = \int_{\mathbb{S}^2} f(\theta,\phi)\, \frac{Y^*_{\ell m}(\theta_R,\phi)}{[\lambda(R,\theta_R)]^{-1/p}}\ \mathrm{d}\Omega(\theta_R,\phi)\,,$$

from which (9) follows by noting $\mathrm{d}\Omega(\theta_R,\phi) = [\lambda(R,\theta_R)]^{-1}\, \mathrm{d}\Omega(\theta,\phi)$. ■

C. Filtering on the sphere

Filtering on the sphere is performed analogously to filtering on the plane; it is the *spherical* convolution of the filter kernel with the analysed signal. The analogue of translations on the sphere are rotations, thus the filtered field is given by the directional spherical convolution

$$F(\rho,R,p) = \int_{\mathbb{S}^2} f(\omega)\, [\mathcal{R}(\rho)\Psi_{R,p}]^*(\omega)\ \mathrm{d}\Omega(\omega)\,, \quad (10)$$

where $\Psi \in L^2(\mathbb{S}^2,\, \mathrm{d}\Omega(\omega))$ is the filter kernel. All orientations in the rotation group $\mathrm{SO}(3)$ are considered, thus directional structure is naturally incorporated. The filter equation (10) is identical to the analysis formula of the continuous wavelet transforms derived on the sphere by [16], [17], hence our fast algorithm to evaluate this equation [18] may be applied to compute the filtered field rapidly. For an example of the directional spherical filtering operation applied to Earth data see [18].

When deriving optimal filters on the sphere it is often convenient to represent the filtering operation in harmonic space. Representing the analysed function and the rotated filter kernel in harmonic space, one may rewrite (10) as

$$F(\rho,R,p) = \sum_{\ell=0}^{\infty} \sum_{m=-\ell}^{\ell} \sum_{m'=-\ell}^{\ell} f_{\ell m} D^{\ell *}_{mm'}(\rho)\, (\Psi_{R,p})^*_{\ell m'}\,. \quad (11)$$

For a filter centred on the north pole the harmonic representation of the filtering operation reduces to

$$F(\mathbf{0},R,p) = \sum_{\ell m} f_{\ell m}\, (\Psi_{R,p})^*_{\ell m}\,, \quad (12)$$

where here and subsequently we use the shorthand notation $\sum_{\ell=0}^{\infty}\sum_{m=-\ell}^{\ell} \equiv \sum_{\ell m}$. Furthermore, for the special case of a filter kernel that is azimuthally symmetric, the filter is dependent on θ only (and not ϕ) and, consequently, the filtered field is independent of the value of γ. In this case, the spherical harmonic coefficients of the filtered field for a particular scale are simply given by

$$[F(R,p)]_{\ell m} = \sqrt{\frac{4\pi}{2\ell+1}}\, f_{\ell m}\, (\Psi_{R,p})^*_{\ell 0}\,. \quad (13)$$

III. Problem Formalisation

In this section we formalise the problem of detecting compact objects embedded in a stochastic background noise process, and propose optimal filtering to enhance the detection of such objects. The formulation given here is similar to that of [12] but is considered in the most general sense, allowing asymmetric templates of various amplitude, position and orientation. Removing the assumption of an azimuthally symmetric template, the case considered in previous works [12], [13], introduces a number of complications as the spherical filtering operation may no longer be represented in harmonic space simply as a product of spherical harmonic coefficients.

A. Formulation

Consider an observed field on the sky $f(\omega)$ consisting of a number of sources $s_i(\omega)$ embedded in a stochastic background process $n(\omega)$. Observations are likely to be made in the presence of additional instrument noise $r(\omega)$ also. The observed field is obtained by measuring (convolving) the actual field with some beam $b(\omega)$. The beam response and instrumental noise may be absorbed into the template and the statistical properties of the background, therefore these components may be included trivially when required. Without loss of generality, the observed field may therefore be represented by

$$f(\omega) = \sum_i s_i(\omega) + n(\omega)\,. \quad (14)$$

Each source may be represented in terms of its amplitude A_i and source profile $s_i(\omega) = A_i\ \tau_i(\omega)$, where $\tau_i(\omega)$ is a dilated and rotated version of the source profile $\tau(\omega)$ of default dilation centred on the north pole,

i.e. $\tau_i(\omega) = \mathcal{R}(\rho_i)\mathcal{D}(R_i, p)\,\tau(\omega)$. One wishes to recover the parameters $\{A_i, R_i, \rho_i\}$ that describe each source amplitude, scale and position/orientation respectively. The stochastic background process is assumed to be a zero-mean $E\left[n(\omega)\right] = 0$, homogeneous and isotropic Gaussian random field, fully characterised by the spectrum

$$E\left[n_{\ell m} n^*_{\ell' m'}\right] = \delta_{\ell\ell'}\delta_{mm'}\, C_\ell \,, \tag{15}$$

where $E\left[\cdot\right]$ denotes the expectation operator. To facilitate the detection of compact sources, the observed field is filtered using (10) to enhance the source contribution relative to the background noise process. The choice of filter kernels that are in some sense optimal is addressed next.

B. Filter constraints

Various optimal filters may be defined by imposing different constraints on the filtered field. Without loss of generality, we derive optimal filters for the detection of a single source located at the north pole (hence we drop the i subscript that denotes source index). Sources located at other positions and orientations are found by rotating the optimal filter, *i.e.* by considering filtered field coefficients over $\mathrm{SO}(3)$.

The following filter characteristics may be imposed when constructing optimal filters:

(i) Unbiased: The filtered field is an unbiased estimator of the source amplitude at the source position, *i.e.* $E\left[F(\mathbf{0}, R, p)\right] = A$.
(ii) Minimum variance: The filtered field has minimum variance at the source position.
(iii) Local extremum in scale: The expected value of the filtered field has an extremum with respect to scale, *i.e.* $\frac{\partial}{\partial R} E\left[F(\mathbf{0}, R, p)\right] = 0$ at $R = R_0$.

Imposing criteria (i) and (ii) only one obtains the usual MF. Imposing the additional constraint (iii) one obtains the SAF, first introduced on the plane by [6]. This additional constraint imposes an extremum at the unknown scale R_0. In the derivation of the SAF this unknown scale drops out and the final filter expressions are independent of R_0. The additional constraint imposed when constructing the SAF provides a means to estimate unknown source scales by checking for a maximum in scale but at a cost of reduced gain. This issue is discussed in more detail in Section IV-D.

C. Filtered field statistics

In order to derive optimal filters on the sphere it is necessary to determine first expressions for the mean and variance of the filtered field at the source position. The filtered field mean at the source position is given by

$$E\left[F(\mathbf{0}, R, p)\right] = A \sum_{\ell m} \tau_{\ell m} \left(\Psi_{R,p}\right)^*_{\ell m} \,. \tag{16}$$

The filtered field variance at the source position is given by

$$\sigma^2_F(\mathbf{0}, R, p) = E\left[|F(\mathbf{0}, R, p)|^2\right] - \left|E\left[F(\mathbf{0}, R, p)\right]\right|^2 . \tag{17}$$

The first term becomes

$$E\left[|F(\mathbf{0}, R, p)|^2\right] = \left|E\left[F(\mathbf{0}, R, p)\right]\right|^2 + \sum_{\ell m} C_\ell \left|\left(\Psi_{R,p}\right)_{\ell m}\right|^2 ,$$

where we have relied on the fact that the stochastic noise process has zero mean and is homogeneous and isotropic. The variance is therefore given by

$$\sigma^2_F(\mathbf{0}, R, p) = \sum_{\ell m} C_\ell \left|\left(\Psi_{R,p}\right)_{\ell m}\right|^2 . \tag{18}$$

The filtered field variance at the source position is also used to determine the error on amplitude estimates.

IV. Optimal Filters

In this section we derive the MF and SAF on the sphere for an arbitrary template profile. The extension of optimal filter theory to the sphere has been derived already by [12] for the special case of azimuthally symmetric source profiles. We re-derive optimal filter theory on the sphere here, making the extension to the more general class of non-azimuthally symmetric source profiles and filters. In addition, we generalise to L^p-norm preserving dilations in order to highlight some minor amendments to previous works. We show that the resultant optimal filters reduce to the expected definitions for azimuthally symmetric template profiles and also that, in the flat, continuous limit, these forms reduce to the optimal filter definitions derived on the plane. To conclude this section we compare the performance of the MF and SAF on the sphere and discuss the relative merits of each filter.

A. Matched filter

Theorem 1: The optimal MF defined on the sphere is obtained by imposing criteria (i) and (ii) defined in Section III-B, *i.e.* by solving the constrained optimisation problem:

$$\min_{\text{w.r.t. } \left(\Psi_{R,p}\right)_{\ell m}} \sigma^2_F(\mathbf{0}, R, p)$$

such that

$$E\left[F(\mathbf{0}, R, p)\right] = A \,. \tag{19}$$

The spherical harmonic coefficients of the resultant MF are given by

$$\left(\Psi_{R,p}\right)_{\ell m} = \frac{\tau_{\ell m}}{a\, C_\ell} \,, \tag{20}$$

where

$$a = \sum_{\ell m} C_\ell^{-1} |\tau_{\ell m}|^2 \,. \tag{21}$$

□

Proof: See Appendix II. ■

A measure of the capability of an optimal filter to detect an embedded source is given by the *maximum detection level*, defined by

$$\Gamma \equiv \frac{E\left[F(\mathbf{0}, R, p)\right]}{\sigma_{F,\min}(\mathbf{0}, R, p)} \,. \tag{22}$$

The minimum variance of the filtered field is found by substituting the expression for the MF given by (20) into (18). One finds that the MF filtered field minimum variance is given by $\sigma^2_{F,\min}(\mathbf{0}, R, p) = a^{-1}$, thus the maximum detection level for the MF is

$$\Gamma_{\mathrm{MF}} = a^{1/2}\, A \,. \tag{23}$$

B. Scale adaptive filter

To construct the optimal SAF defined on the sphere we first recast criterion (iii) in a form expressed in terms of the filter spherical harmonic coefficients and *not* the coefficients of the differentiated filter. A suitable form is given by the following lemma.

Lemma 2: Optimal filter criterion (iii), imposing a local extremum in scale, may be recast in the following more applicable form:

$$\sum_{\ell m} (\Psi_{R_0,p})^*_{\ell m}(A_{\ell p}\tau_{\ell m} - B_{\ell m}\tau_{\ell-1,m}) = 0\,, \qquad (24)$$

where $A_{\ell p} \equiv \ell + 2/p - 1$ and $B_{\ell m} \equiv (\ell^2 - m^2)^{1/2}$. □

The proof of this lemma may be found in [19] (the proof is not repeated here since it requires multiple pages). It is now possible to derive the following theorem, the definition of the optimal SAF defined on the sphere.

Theorem 2: The optimal SAF defined on the sphere is obtained by imposing criteria (i), (ii) and (iii) defined in Section III-B, *i.e.* by solving the constrained optimisation problem:

$$\min_{\text{w.r.t. } (\Psi_{R_0,p})_{\ell m}} \sigma^2_F(\mathbf{0}, R, p)$$

such that

$$E\left[F(\mathbf{0}, R, p)\right] = A \qquad (25)$$

and

$$\frac{\partial}{\partial R} E\left[F(\mathbf{0}, R, p)\right]\bigg|_{R=R_0} = 0\,. \qquad (26)$$

The spherical harmonic coefficients of the resultant SAF are given by

$$(\Psi_{R_0,p})_{\ell m} = \frac{c\tau_{\ell m} - b(A_{\ell p}\tau_{\ell m} - B_{\ell m}\tau_{\ell-1,m})}{\Delta C_\ell}\,, \qquad (27)$$

where

$$b = \sum_{\ell m} C_\ell^{-1}\tau_{\ell m}(A_{\ell p}\tau^*_{\ell m} - B_{\ell m}\tau^*_{\ell-1,m})\,, \qquad (28)$$

$$c = \sum_{\ell m} C_\ell^{-1}\left|A_{\ell p}\tau_{\ell m} - B_{\ell m}\tau_{\ell-1,m}\right|^2\,, \qquad (29)$$

$$\Delta = ac - |b|^2 \qquad (30)$$

and a is defined by (21). □

Proof: See Appendix III. ■

The minimum variance of the filtered field is found by substituting the expression for the SAF given by (27) into (18). One finds that the SAF filtered field minimum variance is given by $\sigma^2_{F,\min}(R_0, p, \mathbf{0}) = c\Delta^{-1}$, thus the maximum detection level for the SAF is

$$\Gamma_{\text{SAF}} = c^{-1/2}\Delta^{1/2}A\,. \qquad (31)$$

C. Azimuthally symmetric case

In this subsection we show that the expressions derived above for arbitrary template profiles reduce to the forms expected for azimuthally symmetric templates (the case considered by [12]). The spherical harmonic coefficients of azimuthally symmetric functions on the sphere are non-zero for $m = 0$ only, hence the general filter expressions that we derive for a directional template should reduce to the symmetric result when setting $m = 0$. The definition of the filter variables used herein differ slightly to those defined by [12] (which we denote by a', b', c' and Δ'). The relationships between these sets of variables are stated in [19]. For now we simply note that all filter variables are identical for $p = 2$, however the case $p = 1$ is adopted by [12]. Simplifying the formula for the MF given by (20) to the azimuthally symmetric setting, one finds that the resulting expression is identical to that derived by [12]. Simplifying the formula for the SAF given by (27) in a similar manner, one obtains the following expression for the SAF of a symmetric template:

$$(\Psi_{R,p})_{\ell 0} = (\Delta' C_\ell)^{-1}\tau_{\ell 0}\left[A_{0p}b'^* + c' - (A_{0p}a' + b')\frac{\text{dln}\tau_{\ell 0}}{\text{dln}\ell}\right].$$

It is apparent that the A_{0p} coefficient of the first b' and of a' are in general dependent on the choice of the L^p-norm preserved by the dilation. For $p = 1$, the case considered by [12], one finds $A_{01} = 1$, not two as given in [12]. When we repeat the derivation of the SAF for the azimuthally symmetric case given by [12] explicitly, we also get a unity term rather than a factor of two for these coefficients, and hence correct an algebraic error in [12]. The forms derived herein for the MF and SAF on the sphere of a directional template therefore reduce to the correct forms derived directly for an azimuthally symmetric template. Moreover, in the flat, continuous limit, the azimuthally symmetric optimal filters derived on the sphere reduce to the forms derived previously on the plane (to make a comparison see, respectively, *e.g.* eqn. (21) of [5] and eqn. (10) of [6]).

D. Comparison

The relative merits of the MF and SAF are compared in this subsection. Recently, the advantages of the SAF (on the plane) have been questioned [10], although these concerns have been refuted by the original proponents of the SAF [6], [7]. We hope to clarify this debate by suggesting that in the ideal case the SAF may not provide a theoretical advantage, however in practice the SAF may indeed prove advantageous.

The SAF filter imposes an extremum in scale in the filtered field and thus must satisfy an additional constraint to the MF. Consequently, the gain of the SAF must be lower than that of the MF. One may show this analytically by comparing the ratio of the detection levels derived in the preceding sections for each optimal filter:

$$\frac{\Gamma_{\text{SAF}}}{\Gamma_{\text{MF}}} = \sqrt{1 - \frac{|b|^2}{ac}}\,. \qquad (32)$$

Filter variables a and c are real and are strictly positive always, consequently (32) is less than one always.

As the gain of the SAF is lower than the gain of the MF one would hope that the SAF provides some other advantage. This is indeed the case when the scale of the source template is unknown. When the source size is unknown the observed field may be filtered at a range of candidate scales. It is then possible, at the source position, to trace the value of the filtered field over scales. The SAF imposes a peak (with respect to scale) in the filtered field that may then be related, either analytically or numerically, to the unknown size of the source template. The drop in gain provided by the SAF is therefore offset by the ability to determine the unknown size of the source.

It has been argued that it is also possible to estimate an unknown template size using the MF [10], in which case the SAF would not provide any advantage. For the MF, it may be possible to relate the filtered field curve (with respect to scale) to the unknown scale of the template. By fitting the entire curve one could therefore directly estimate the source scale, although this curve is unlikely to have a local peak. In practice it is much easier to determine a peak in the filtered field (the SAF approach to estimating source size), than try to fit a curve to the field (the MF approach to estimating source size). The amplitude of the source is unknown also, hence it is only the curvature of the curve that one may fit and curvature changes much more rapidly about an extremum. It is therefore clear that the SAF does indeed provide some practical advantages to the MF when the scale of the source profile is unknown.

V. Simulations

We apply the optimal filter theory derived in the preceding section to the detection of compact objects from simulated data. A very simple detection strategy is adopted. The development of more sophisticated detection strategies, a rigorous quantification of the performance of the resulting object detection and the application to real data is the subject of future work. The motivation here is to demonstrate the theory with a very simple example only.

A. Optimal filters

We construct examples of optimal filters defined on the sphere using the filter expressions derived in Section IV. Our ultimate aim is to apply filters to detect compact objects embedded in CMB data, such as the recent observations made by the NASA Wilkinson Microwave Anisotropy Probe (WMAP) [1]. Optimal filters are therefore constructed here in an analogous simulated setting. The CMB power spectrum that best fits the WMAP data is used to model the stochastic background process, with a Gaussian beam of full-width-half-maximum (FWHM) of $13'$ applied. Isotropic white noise of constant variance $0.05(\mathrm{mK})^2$ is added to reflect the noise in WMAP observations. We consider the construction in this setting of the MF and SAF for the directional butterfly template illustrated in Figure 2 (a) (the butterfly template is defined by the partial derivative in one direction only of a two-dimensional Gaussian on the sphere; see [18] for a definition).[2] The resultant MF and SAF are illustrated in Figure 2 (b) and (c) respectively. Optimal filters are constructed here in the context of L^2-norm preserving dilations, *i.e.* for $p = 2$. Furthermore, in practice the template profiles are assumed to be band-limited at $\ell_{\max}$, in which case all expressions and summations involving ℓ are computed up to $\ell_{\max}$ only. In these experiments we choose $\ell_{\max} = 256$ since this is a more than adequate band-limit to ensure that all structure of the butterfly profile is considered.

A Fortran 90 package called `S2FIL`[3] ($\mathbb{S}^2$ FILtering) has been implemented to compute the equations describing the MF and SAF defined by Theorem 1 and Theorem 2 respectively. This package makes use of our `FastCSWT`[3] package [18] to perform fast filtering on the sphere. Additional numerical considerations must be taken into account when implementing the filter equations since they often involve dividing the template spherical harmonics by the power spectrum of the background process, which becomes problematic when taking the ratio of two very small numbers. These considerations are discussed in detail in [19].

B. Object detection

To demonstrate optimal filter theory applied to object detection a simple example is considered. Although the optimal filters we have derived may be used to detect objects of unknown size, in this simple demonstration we consider only a butterfly template of a fixed, known size. Since the template size is known only the MF on the sphere is applied. The MF is applied to simulations of the CMB with artificially embedded butterfly sources, in order to recover the positions, orientations and amplitudes of the sources. Firstly, the simulation pipeline used to construct this data is described. The object detection procedure is then described briefly, before the results obtained from applying this procedure to simulated data are presented.

1) Simulation pipeline: To test the application of optimal filters on the sphere to object detection, simulated data where the ground truth is known is analysed. We have implemented a Fortran 90 package called `COMB`[3] (COmpact eMBedded object simulations) to facilitate such simulations. `COMB` allows the user to embed compact functions on the sphere within a stochastic background process. The parameters of the embedded objects are uniformly sampled from some prescribed interval, whereas the background process is specified by its power spectrum. Functionality is also included to incorporate noise and beams.

An example of maps simulated using `COMB` is shown in the first four panels of Figure 3. In this example the background process is described by the best-fit WMAP CMB power spectrum, a beam of $13'$ FWHM is applied and isotropic white noise of variance $0.05(\mathrm{mK})^2$ is added (the same setting in which the optimal filters discussed in Section V-A were constructed). A map of simulated butterfly sources is shown in Figure 3 (c) and is embedded in the resultant simulated

[2]The step of the butterfly template may be used to model the line-like discontinuity of Kaiser-Stebbins type cosmic string signatures [3].

[3]The `S2FIL`, `FastCSWT` and `COMB` packages are available for download from `http://www.mrao.cam.ac.uk/~jdm57/`. These packages require the `HEALPix` (`http://healpix.jpl.nasa.gov/`) [20] and `FFTW` (`http://www.fftw.org/`) libraries.

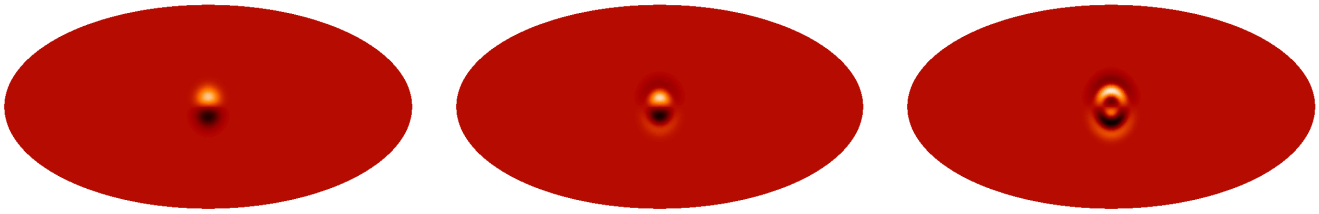

(a) Butterfly template (b) MF (c) SAF

Fig. 2. Optimal filters for the butterfly template constructed on the sphere in the setting consistent with WMAP observations (see text). (Functions/data defined on the sphere are illustrated here and subsequently using the Mollweide projection.)

map shown in Figure 3 (d). In this situation the signal-to-noise ratio (SNR) of an embedded object is defined by the ratio of the peak amplitude of the template relative to the root-mean-squared (RMS) value of the CMB background. For the butterfly templates it can be shown that $\mathrm{SNR} \approx 0.4A$, where A is the amplitude of the object (note that the butterfly template definition is normalised, with a peak amplitude of 0.13mK for $A = 1.0$). In the example illustrated in Figure 3 all objects have a constant amplitude of $A = 1.0$, corresponding to $\mathrm{SNR} = 0.40$. Moreover, in this simulation all embedded objects have the same orientation ($\gamma = 0°$); that is, the orientation of the objects are aligned to point to the north pole. This is a useful test case since it reduces the complexity of the subsequent object detection to that of a symmetric template profile, while still adopting the more general optimal filter definitions. In the following object detection we also consider simulations where the orientations of the objects vary, however object orientations are only allowed to lie on a discrete, uniformly sampled grid with $N_\gamma = 5$ samples. By restricting the allowable orientations to a grid it is necessary only to compute the filtered field for a small number of orientations. Obviously in practice object orientations will not lie on a grid, however in this case one may simply compute the filtered field for a higher orientation resolution (or one may use steerable filters[4] to extract the orientation corresponding to the most dominant feature, thereby effectively considering all continuous orientations; this is the topic of future work). An orientational resolution of $N_\gamma = 5$ is sufficient for the simple demonstration presented here.

2) Detection procedure: For the purpose of this demonstration we perform only a naive detection strategy based on thresholding the filtered field. Firstly the initial map is filtered using the MF to enhance the contribution due to the embedded sources relative to the background. The local maxima of the filtered field that lie above a certain threshold are used to define detected objects. The filtered field is thresholded at a level determined by a constant (N_σ) times the standard deviation of the map. Typically an N_σ of 2.5 or 3.0 is used. The magnitude and position of each local maximum that remains in the thresholded field is used to compute the parameters of detected sources. This object detection procedure is implemented in the `S2FIL` package.

This detection algorithm is applied to the simulated data illustrated in Figure 3. The filtered field is displayed in Figure 3 (e) and the objects recovered from the local maxima of the filtered field are shown in Figure 3 (f). Notice that for this simulation at $\mathrm{SNR} = 0.40$ all embedded objects are recovered accurately and no false detections are made. We now consider more difficult object detection problems.

[4]Steerable template functions yield steerable optimal filters on the sphere since the filter equations do not mix m structure. See [17] for a discussion of steerable filters on the sphere.

TABLE I

OBJECT DETECTION PERFORMANCE FOR $\gamma = 0°$

SNR	N_σ	Detections Correct	Detections False	Number of sources
0.40	3.0	10	0	10
0.40	2.5	10	1	10
0.25	3.0	6	0	10
0.25	2.5	8	2	10
0.20	3.0	5	0	10
0.20	2.5	7	6	10

3) Results: The example illustrated in Figure 3 demonstrates object detection on the sphere for a relatively easy case. By considering more difficult detection situations we examine the limits of the simple detection algorithm described above. Firstly, only a single fixed orientation is considered, before the orientation of embedded objects is allowed to vary.

For objects of known orientation we examine the effect of reducing the SNR of the embedded sources on the number of successful and false detections. We also experiment with thresholding levels $N_\sigma = 3.0$ and $N_\sigma = 2.5$. The results of these tests are given in Table I. To ensure minimal false detections are made one should threshold at $N_\sigma = 3.0$, however to improve the completeness of positive detections one may use $N_\sigma = 2.5$, at the expense of a small number of false detections.

We now consider objects with an unknown orientation laying on a uniform grid of resolution $N_\gamma = 5$. Allowing orientations to vary introduces an extra degree-of-freedom and thus makes the object detection problem more difficult. At $\mathrm{SNR} = 0.40$, for thresholding levels $N_\sigma = 3.0$ and $N_\sigma = 2.5$, of ten embedded objects we recover six and eight objects correctly and make zero and one false detection respectively. At $\mathrm{SNR} = 0.25$ we recover five objects correctly and make one false detection for $N_\sigma = 3.0$ ($N_\sigma = 2.5$ is not appropriate for this low SNR). Finally, we demonstrate in this setting the recovery of objects at a range of different amplitudes. The actual and recovered object parameters are described in Table II and may be observed in Figure 4. One sigma errors on the amplitude estimates are calculated from the variance of the filtered field at the source position (as discussed in

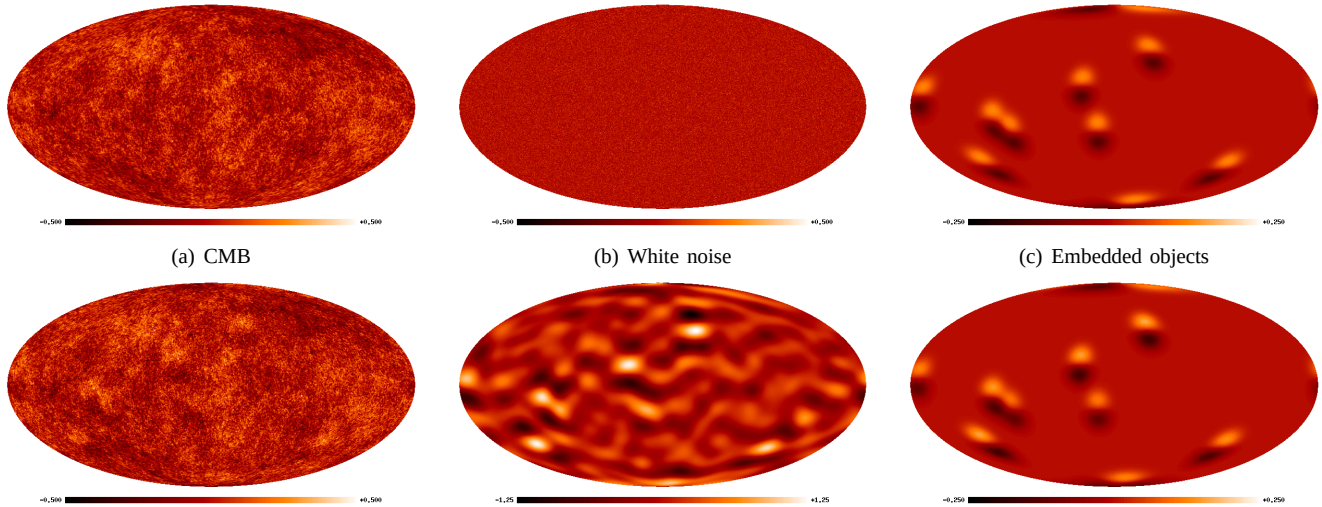

(a) CMB (b) White noise (c) Embedded objects

(d) Simulated sky with objects embedded (e) Filtered field (f) Recovered objects

Fig. 3. Embedded object simulation and recovered objects. The CMB background shown in panel (a) is simulated in accordance with the CMB power spectrum consistent with current observations, noise of variance $0.05(\text{mK})^2$ (panel (b)) is added and a beam of $13'$ FWHM is applied. The simulated butterfly templates ($\text{SNR} = 0.40$) shown in panel (c) are embedded in the the resultant simulated map shown in panel (d). The MF filtered field of the simulated sky is shown in panel (e). The local maxima in the filtered field are detected by thresholding at $N_\sigma = 3.0$ to recover the compact objects depicted in panel (f). In this example all embedded objects are detected and no false detections are made. (All maps shown here and subsequently are displayed in units of mK.)

Section III-C).

It is important to note that the detection strategies demonstrated here are extremely naive and are presented merely to demonstrate the new filter framework derived on the sphere. A more rigorous approach is to perform more sophisticated detection classification schemes, such as the Neyman-Pearson test. Moreover, for certain classes of template functions which are steerable, one may use steerable filters to extract a single orientation over the domain of all continuous orientations. This is expected to improve considerably the performance of object detection in cases of varying source orientation, to the extent that one would expect the performance to match that of cases where the source orientation is known. These extensions are the focus of future work.

TABLE II

ACTUAL AND RECOVERED OBJECT PARAMETERS

Source	Object parameters	
	Amplitude	Euler angles
1	$A = 1.48$	$(\alpha, \beta, \gamma) = (15.0^\circ, 108.3^\circ, 72.0^\circ)$
	$\hat{A} = 1.66 \pm 0.20$	$(\hat{\alpha}, \hat{\beta}, \hat{\gamma}) = (14.7^\circ, 107.9^\circ, 72.0^\circ)$
2	$A = 1.06$	$(\alpha, \beta, \gamma) = (29.2^\circ, 75.4^\circ, 0.0^\circ)$
	$\hat{A} = 1.26 \pm 0.20$	$(\hat{\alpha}, \hat{\beta}, \hat{\gamma}) = (30.9^\circ, 75.6^\circ, 0.0^\circ)$
3	$A = 1.43$	$(\alpha, \beta, \gamma) = (78.4^\circ, 0.7^\circ, 288.0^\circ)$
	Not recovered	
4	$A = 1.19$	$(\alpha, \beta, \gamma) = (94.4^\circ, 109.1^\circ, 216.0^\circ)$
	$\hat{A} = 1.34 \pm 0.20$	$(\hat{\alpha}, \hat{\beta}, \hat{\gamma}) = (92.6^\circ, 109.3^\circ, 216.0^\circ)$
5	$A = 0.81$	$(\alpha, \beta, \gamma) = (107.8^\circ, 99.6^\circ, 144.0^\circ)$
	Not recovered	
6	$A = 1.13$	$(\alpha, \beta, \gamma) = (136.0^\circ, 133.9^\circ, 144.0^\circ)$
	Not recovered	
7	$A = 0.93$	$(\alpha, \beta, \gamma) = (172.3^\circ, 82.7^\circ, 144.0^\circ)$
	$\hat{A} = 1.25 \pm 0.20$	$(\hat{\alpha}, \hat{\beta}, \hat{\gamma}) = (171.9^\circ, 81.2^\circ, 144.0^\circ)$
8	$A = 0.95$	$(\alpha, \beta, \gamma) = (241.2^\circ, 137.2^\circ, 72.0^\circ)$
	$\hat{A} = 1.02 \pm 0.20$	$(\hat{\alpha}, \hat{\beta}, \hat{\gamma}) = (242.8^\circ, 138.0^\circ, 72.0^\circ)$
9	$A = 1.00$	$(\alpha, \beta, \gamma) = (317.7^\circ, 172.3^\circ, 72.0^\circ)$
	$\hat{A} = 1.76 \pm 0.20$	$(\hat{\alpha}, \hat{\beta}, \hat{\gamma}) = (287.0^\circ, 180.0^\circ, 72.0^\circ)$
10	$A = 1.16$	$(\alpha, \beta, \gamma) = (321.7^\circ, 50.7^\circ, 144.0^\circ)$
	$\hat{A} = 1.08 \pm 0.20$	$(\hat{\alpha}, \hat{\beta}, \hat{\gamma}) = (321.4^\circ, 52.5^\circ, 144.0^\circ)$
11	Not present	
	$\hat{A} = 0.96 \pm 0.20$	$(\hat{\alpha}, \hat{\beta}, \hat{\gamma}) = (47.0^\circ, 67.9^\circ, 72.0^\circ)$

VI. Concluding Remarks

We have extended the concept of optimal filtering to a spherical manifold. Expressions for the spherical MF and SAF have been derived for general non-azimuthally symmetric template objects. For the special case of an azimuthally symmetric template we have shown that the general results derived herein reduce to the forms derived directly in this setting. Moreover, we have also shown that in the flat approximation the optimal filters derived on the sphere reduce to the corresponding optimal filter definitions defined on the plane.

The focus of this paper is to derive optimal filter theory on the sphere, nevertheless we have also demonstrated the application of optimal filters to simple object detection. We have generated simulations on the sphere of objects embedded in a stochastic background process. Using this simulated data we have tested a simple object detection algorithm based on thresholding the optimal filtered field. This simple object detection strategy has been demonstrated to perform well, even at low SNR.

In the future we intend to develop more sophisticated detection classification schemes using the optimal filtered field. Moreover, for steerable template profiles the use of steerable optimal filters is expected to improve considerably the performance of object detection in cases of varying source orientation. We intend to then apply the resulting object detection algorithms to real CMB data to search for cosmic string signatures, a theoretically postulated but as yet unobserved phenomenon [3].

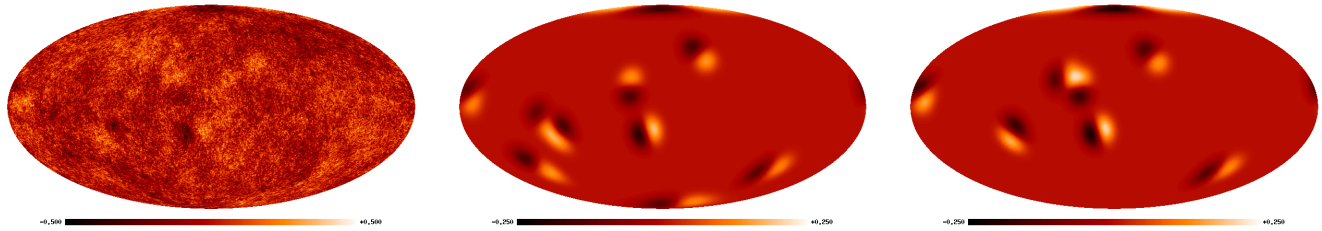

(a) Simulated sky with objects embedded (b) Actual objects (c) Recovered objects

Fig. 4. Embedded object simulation and recovered objects for a range of SNRs, $N_\gamma = 5$ and $N_\sigma = 2.5$. See Table II for the actual and recovered parameters of the embedded sources.

Appendix I
Proof of Dilation Definition (Definition 1)

We prove that the definition of an L^p-norm preserving spherical dilation does indeed preserve the L^p-norm. The result for the case $p = 2$ is given by [16] and an explicit proof is given by [17]. For all practical purposes only the cases $p = \{1, 2, \infty\}$ are considered, nevertheless we prove the result for all positive integer p, taking a different approach to that of [17]. First consider the case of positive integer $p < \infty$. One requires $\|\mathcal{D}_p(R)f\|_p = \|f\|_p$, or equivalently $I_1 = I_2$, where $I_1 = \int_{\mathbb{S}^2} |f(\theta,\phi)|^p \, \mathrm{d}\Omega(\theta,\phi)$ and $I_2 = \int_{\mathbb{S}^2} |\left[\lambda(R,\theta)\right]^{1/p} f(\theta_{1/R},\phi)|^p \, \mathrm{d}\Omega(\theta,\phi)$. By making a change of variables I_2 may be rewritten as

$$I_2 = \int_{\mathbb{S}^2} |f(\theta,\phi)|^p |\lambda(R,\theta_R)| \sin\theta_R \, R \, \frac{\cos^2(\theta_R/2)}{\cos^2(\theta/2)} \, \mathrm{d}\theta \, \mathrm{d}\phi \, .$$

Thus, for $I_1 = I_2$ it is apparent, after a little algebra, that the cocycle required to preserve the L^p-norm (for positive integer $p < \infty$) is of the form given by (7). Now consider the L^∞-norm case, corresponding to the case where no cocycle term is applied. When no cocycle is applied the function is dilated only and is not scaled, hence the maximum absolute value of the function over its domain remains unaltered. Consequently, the infinity norm is also preserved.

Appendix II
Proof of MF Theorem (Theorem 1)

We solve the MF optimisation problem by minimising the Lagrangian

$$\mathcal{L} = \sum_{\ell m} C_\ell \, \left|(\Psi_{R,p})_{\ell m}\right|^2 + \mu_1 \, \mathrm{Re}\left[\sum_{\ell m} \tau_{\ell m} \, (\Psi_{R,p})^*_{\ell m} - 1\right] + \mu_2 \, \mathrm{Im}\left[\sum_{\ell m} \tau_{\ell m} \, (\Psi_{R,p})^*_{\ell m}\right] \, ,$$

where μ_1 and μ_2 are Lagrange multipliers. Notice that the real and imaginary parts of the constraint are made explicit. To solve this problem the filter and template spherical harmonic coefficients are represented in terms of their real and imaginary parts: let $(\Psi_{R,p})_{\ell m} = a_{\ell m} + \mathrm{i} b_{\ell m}$ and $\tau_{\ell m} = c_{\ell m} + \mathrm{i} d_{\ell m}$. To minimise the Lagrangian one requires

$$\frac{\partial \mathcal{L}}{\partial a_{\ell m}} = 2 C_\ell \, a_{\ell m} + \mu_1 c_{\ell m} + \mu_2 d_{\ell m} = 0$$

and

$$\frac{\partial \mathcal{L}}{\partial b_{\ell m}} = 2 C_\ell \, b_{\ell m} + \mu_1 d_{\ell m} - \mu_2 c_{\ell m} = 0 \, ,$$

plus the original constraints specified by (19) (one for the real and one for the imaginary component). Solving these equations simultaneously, one finds $\mu_1 = -2a^{-1}$ and $\mu_2 = 0$ for the Lagrange multipliers and $a_{\ell m} = a^{-1} C_\ell^{-1} c_{\ell m}$ and $b_{\ell m} = a^{-1} C_\ell^{-1} d_{\ell m}$ for the real and imaginary parts of the filter spherical harmonic coefficients, where a is defined by (21). Thus, the spherical harmonic coefficients of the optimal MF on the sphere are given by $(\Psi_{R,p})_{\ell m} = a^{-1} C_\ell^{-1} \tau_{\ell m}$.

The extremum found is checked to ensure it is a minimum. The second derivatives of the Lagrangian are $\mathcal{L}_{aa} = 2C_\ell$, $\mathcal{L}_{bb} = 2C_\ell$ and $\mathcal{L}_{ab} = 0$, where the subscript notation for partial derivatives is used. Now $\mathcal{L}_{ab}^2 < \mathcal{L}_{aa}\mathcal{L}_{bb}$ and both $\mathcal{L}_{aa} > 0$ and $\mathcal{L}_{bb} > 0$, hence a minimum has indeed been found.

Appendix III
Proof of SAF Theorem (Theorem 2)

We solve the SAF optimisation problem by minimising the Lagrangian

$$\begin{aligned}\mathcal{L} = &\sum_{\ell m} C_\ell \, \left|(\Psi_{R_0,p})_{\ell m}\right|^2 + \mu_1 \, \mathrm{Re}\left[\sum_{\ell m} \tau_{\ell m} \, (\Psi_{R_0,p})^*_{\ell m} - 1\right] \\ &+ \mu_2 \, \mathrm{Im}\left[\sum_{\ell m} \tau_{\ell m} \, (\Psi_{R_0,p})^*_{\ell m}\right] \\ &+ \mu_3 \, \mathrm{Re}\left[\sum_{\ell m} (\Psi_{R_0,p})^*_{\ell m} (A_{\ell p}\tau_{\ell m} - B_{\ell m}\tau_{\ell-1,m})\right] \\ &+ \mu_4 \, \mathrm{Im}\left[\sum_{\ell m} (\Psi_{R_0,p})^*_{\ell m} (A_{\ell p}\tau_{\ell m} - B_{\ell m}\tau_{\ell-1,m})\right] \, ,\end{aligned}$$

where μ_1, μ_2, μ_3 and μ_4 are Lagrange multipliers. Notice that the real and imaginary parts of each constraint are again made explicit. To solve this problem the filter and template spherical harmonic coefficients are represented in terms of their real and imaginary parts: let $(\Psi_{R_0,p})_{\ell m} = a_{\ell m} + \mathrm{i} b_{\ell m}$ and $\tau_{\ell m} = c_{\ell m} + \mathrm{i} d_{\ell m}$. To minimise the Lagrangian one requires

$$\begin{aligned}\frac{\partial \mathcal{L}}{\partial a_{\ell m}} = &\, 2C_\ell a_{\ell m} + \mu_1 c_{\ell m} + \mu_2 d_{\ell m} \\ &+ \mu_3 (A_{\ell p} c_{\ell m} - B_{\ell m} c_{\ell-1,m}) \\ &+ \mu_4 (A_{\ell p} d_{\ell m} - B_{\ell m} d_{\ell-1,m}) = 0 \qquad (33)\end{aligned}$$

and

$$\begin{aligned}\frac{\partial \mathcal{L}}{\partial b_{\ell m}} =& 2C_\ell b_{\ell m} + \mu_1 d_{\ell m} - \mu_2 c_{\ell m} \\ &+ \mu_3 (A_{\ell p} d_{\ell m} - B_{\ell m} d_{\ell-1,m}) \\ &- \mu_4 (A_{\ell p} c_{\ell m} - B_{\ell m} c_{\ell-1,m}) = 0 \,, \end{aligned} \tag{34}$$

plus the original constraints specified by (25) and (26). Using (33) and (34) it is possible to eliminate $a_{\ell m}$ and $b_{\ell m}$ from the original constraints, yielding a system of linear equations for the Lagrange multipliers that depend on the template spherical harmonic coefficients only. Solving this system one finds $[\mu_1, \mu_2, \mu_3, \mu_4] = \frac{2}{\Delta}[-c, 0, \mathrm{Re}(b), -\mathrm{Im}(b)]$ for the Lagrange multipliers. Substituting the Lagrange multipliers into (33) and (34) one obtains the following expressions for the real and imaginary parts of the filter spherical harmonic coefficients:

$$\begin{aligned} a_{\ell m} = (\Delta C_\ell)^{-1} \big[& c\, c_{\ell m} - \mathrm{Re}(b)(A_{\ell p} c_{\ell m} - B_{\ell m} c_{\ell-1,m}) \\ & + \mathrm{Im}(b)(A_{\ell p} d_{\ell m} - B_{\ell m} d_{\ell-1,m}) \big] \end{aligned}$$

and

$$\begin{aligned} b_{\ell m} = (\Delta C_\ell)^{-1} \big[& c\, d_{\ell m} - \mathrm{Re}(b)(A_{\ell p} d_{\ell m} - B_{\ell m} d_{\ell-1,m}) \\ & - \mathrm{Im}(b)(A_{\ell p} c_{\ell m} - B_{\ell m} c_{\ell-1,m}) \big] \,. \end{aligned}$$

Thus, combining the real and imaginary parts, the spherical harmonic coefficients of the optimal SAF are given by (27).

The extremum found is checked to ensure it is a minimum. The second derivatives of the Lagrangian are $\mathcal{L}_{aa} = 2C_\ell$, $\mathcal{L}_{bb} = 2C_\ell$ and $\mathcal{L}_{ab} = 0$, where the subscript notation for partial derivatives is used. Now $\mathcal{L}_{ab}^2 < \mathcal{L}_{aa}\mathcal{L}_{bb}$ and both $\mathcal{L}_{aa} > 0$ and $\mathcal{L}_{bb} > 0$, hence a minimum has indeed been found.

REFERENCES

[1] G. Hinshaw, M. R. Nolta, C. L. Bennett, R. Bean, O. Doré, M. R. Greason, M. Halpern, R. S. Hill, N. Jarosik, A. Kogut, E. Komatsu, M. Limon, N. Odegard, S. S. Meyer, L. Page, H. V. Peiris, D. N. Spergel, G. S. Tucker, L. Verde, J. L. Weiland, E. Wollack, and E. L. Wright, "Three-year Wilkinson Microwave Anisotropy Probe (WMAP) observations: temperature analysis," *Astrophys. J.*, vol. 170, pp. 288–334, June 2007.

[2] R. A. Sunyaev and Y. B. Zeldovich, "Small-Scale Fluctuations of Relic Radiation," *Astrophys. & Space Science*, vol. 7, pp. 3–+, 1970.

[3] N. Kaiser and A. Stebbins, "Microwave anisotropy due to cosmic strings," *Nature*, vol. 310, pp. 391–393, 1984.

[4] M. Tegmark and A. de Oliveira-Costa, "Removing point sources from CMB maps," *Astrophys. J. Lett.*, vol. 500, pp. L83–L86, 1998.

[5] M. G. Haehnelt and M. Tegmark, "Using the kinematic Sunyaev-Zel'dovich effect to determine the peculiar velocities of clusters of galaxies," *Mon. Not. Roy. Astron. Soc.*, vol. 279, pp. 545–556, 1996.

[6] J. L. Sanz, D. Herranz, and E. Martínez-González, "Optimal detection of sources on a homogeneous and isotropic background," *Astrophys. J.*, vol. 552, pp. 484–492, 2001.

[7] D. Herranz, J. L. Sanz, R. B. Barreiro, and E. Martínez-González, "Scale-adaptive filters for the detection/separation of compact sources," *Astrophys. J.*, vol. 580, pp. 610–625, 2002.

[8] L. Cayón, J. L. Sanz, R. B. Barreiro, E. Martínez-González, P. Vielva, L. Toffolatti, J. Silk, J. M. Diego, and F. Argüeso, "Isotropic wavelets: a powerful tool to extract point sources from cosmic microwave background maps," *Mon. Not. Roy. Astron. Soc.*, vol. 315, pp. 757–761, 2000.

[9] R. B. Barreiro, J. L. Sanz, D. Herranz, and E. Martínez-González, "Comparing filters for the detection of point sources," *Mon. Not. Roy. Astron. Soc.*, vol. 342, pp. 119–133, 2003.

[10] R. Vio, P. Andreani, and W. Wamsteker, "Some good reasons to use matched filters for the detection of point sources in CMB maps," *Astron. & Astrophys.*, vol. 414, pp. 17–21, 2004.

[11] P. Vielva, E. Martínez-González, J. E. Gallegos, L. Toffolatti, and J. L. Sanz, "Point source detection using the spherical Mexican hat wavelet on simulated all-sky Planck maps," *Mon. Not. Roy. Astron. Soc.*, vol. 344, pp. 89–104, 2003.

[12] B. M. Schaefer, C. Pfrommer, R. M. Hell, and M. Bartelmann, "Detecting Sunyaev-Zel'dovich clusters with Planck: II. Foreground components and optimised filtering schemes," *Mon. Not. Roy. Astron. Soc.*, vol. 370, pp. 1713–1736, Aug. 2006.

[13] B. M. Schaefer and M. Bartelmann, "Detecting Sunyaev-Zel'dovich clusters with Planck: III. Properties of the expected SZ-cluster sample," *ArXiv*, 2006.

[14] D. A. Varshalovich, A. N. Moskalev, and V. K. Khersonskii, *Quantum theory of angular momentum*. Singapore: World Scientific, 1989.

[15] T. Risbo, "Fourier transform summation of Legendre series and D-functions," *J. Geodesy*, vol. 70, no. 7, pp. 383–396, 1996.

[16] J.-P. Antoine and P. Vandergheynst, "Wavelets on the 2-sphere: a group theoretical approach," *Applied Comput. Harm. Anal.*, vol. 7, pp. 1–30, 1999.

[17] Y. Wiaux, L. Jacques, and P. Vandergheynst, "Correspondence principle between spherical and Euclidean wavelets," *Astrophys. J.*, vol. 632, pp. 15–28, 2005.

[18] J. D. McEwen, M. P. Hobson, D. J. Mortlock, and A. N. Lasenby, "Fast directional continuous spherical wavelet transform algorithms," *IEEE Trans. Sig. Proc.*, vol. 55, no. 2, pp. 520–529, 2007.

[19] J. D. McEwen, "Analysis of cosmological observations on the celestial sphere," Ph.D. dissertation, University of Cambridge, 2006.

[20] K. M. Górski, E. Hivon, A. J. Banday, B. D. Wandelt, F. K. Hansen, M. Reinecke, and M. Bartelmann, "Healpix – a framework for high resolution discretization and fast analysis of data distributed on the sphere," *Astrophys. J.*, vol. 622, pp. 759–771, 2005.

Jason McEwen was born in Wellington, New Zealand, in August 1979. He received a B.E. (Hons) degree in Electrical and Computer Engineering from the University of Canterbury, New Zealand, in 2002 and a Ph.D. degree in Astrophysics from the University of Cambridge in 2006.

He began a Research Fellowship at Clare College, Cambridge, in 2007. His research interests include wavelets on the sphere, the cosmic microwave background and wavelet based reflectance and illumination in computer graphics.

Michael Hobson was born in Birmingham, England, in September 1967. He received the B.A. degree in Natural Sciences with honours and the Ph.D. degree in Astrophysics from the University of Cambridge, England, in 1989 and 1993 respectively.

Since 1993, he has been a member of the Astrophysics Group of the Cavendish Laboratory at the University of Cambridge, where he has been a Reader in Astrophysics and Cosmology since 2003. His research interests include theoretical and observational cosmology, particularly anisotropies in the cosmic microwave background, gravitation, Bayesian analysis techniques and theoretical optics.

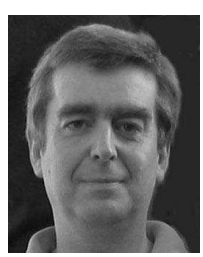

Anthony Lasenby was born in Malvern, England, in June 1954. He received a B.A. then M.A. from the University of Cambridge in 1975 and 1979, an M.Sc. from Queen Mary College, London in 1978 and a Ph.D. from the University of Manchester in 1981.

His Ph.D. work was carried out at the Jodrell Bank Radio Observatory specializing in the Cosmic Microwave Background, which has been a major subject of his research ever since. After a brief period at the National Radio Astronomy Observatory, Tucson, Arizona, he moved from Manchester to Cambridge in 1984, and has been at the Cavendish Laboratory Cambridge since then. He is currently Head of the Astrophysics Group and the Mullard Radio Astronomy Observatory of the Cavendish Laboratory. His other main interests include theoretical physics and cosmology, the application of new geometric techniques in computer graphics and electromagnetic modelling, and statistical techniques in data analysis.